Bifurcation and chaos of a density dependent Leslie population model

Guo Feng[1]   Song Xinghao[1]

[1]School of Data and Computer Science, Shandong Women's University, Jinan, China 250300

Email: sdwugf@163.com

Abstract: A discrete-time Leslie model with Hassell growth function for two generations is investigated by qualitative analysis and numerical simulation. Local stability analysis of the system is carried out. Many forms of complex dynamics are observed, including chaotic bands with periodic windows, flip bifurcations, and Hopf bifurcations, attractor crises, and non-unique dynamics (meaning that several attractors coexist). Numerical simulation results not only show the consistence with the theoretical analysis but also display the new and interesting dynamical behaviors, including different periodic orbits in chaotic regions, attracting invariant circle, period-doubling bifurcations from stable equilibriums leading to chaos, interior crisis and boundary crisis. The largest Lyapunov exponents are numerically computed to confirm further the complexity of these dynamic behaviors. The analysis and results in this paper are interesting in mathematics and biology.

Keywords: discrete-time Hassell model; Hopf bifurcation; chaotic attractor; numerical simulation.

1. Introduction

In 1964, Hénon took KAM Theorem as the background, and found that there was deterministic random behavior in two-dimensional non-integrable Hamiltonian system, that is claimed Hénon attractor. Ruelle and Takens proposed the concept of "strange attractor", which promoted the research of Smale horseshoe attractor (Smale, 1976). Lorenz (1963) pointed out that there must be a connection between the inexact recurrence of climate and the inability of long-term weather forecast. It is found that the chaos phenomenon is "extremely sensitive to the initial conditions".

The word "chaos" is formally used by Li and Yorke (1975), which is considered as the first formal expression of chaos theory. Smale (1976) gave an example of horseshoe mapping, which opened the mathematical method of studying chaos. LaSota (1981) studied the initial value problem of the first order nonlinear partial differential equation of the wormhole model. Brunovsky (1983) gave the definition of chaotic mapping.

In population dynamics, there are two kinds of mathematical models: the continuous-time models described by differential equations or dynamical systems, and the discrete-time models described by difference equations, discrete dynamical systems or iterative mappings. The simplest continuous-time population model is the logistic differential equation of a single species, first introduced by Verhulst (1838) and later studied further by Pearl and Reed (1920):

$$\dot{x} = r_0 x \left(1 - \frac{x}{k} \right) \tag{1}$$

where $x(t)$ denotes the population of a single species at time t, k is the carrying capacity of the population, and r_0 is the intrinsic growth rate. Eq. (1) describes the growth rate of the population size of a single species. However, the population size of a single species may has a fixed interval between generations or possibly a fixed interval between measurements. For example, many species of insect have no overlap between successive generations, and thus their population evolves in discrete-time steps. Such a population dynamics is described by a sequence $\{x_n\}$ that can be modeled by the logistic difference equation

$$x_{n+1} = x_n + r_0 x_n \left(1 - \frac{x_n}{k} \right) \tag{2}$$

We can see that Eq. (2) is time discretization of Eq. (1) by the forward Euler scheme with step one.

May (1976) made the profound discovery in the 1970s that several discrete-time models used

to describe the dynamics of isolated single-species populations display chaotic behavior for large ranges of parameter values. Furthermore, an early work by Beddington (1975) showed that discrete-time host–parasitoid models can produce a much richer set of dynamic patterns than those observed in continuous-time models, where the dynamics include only stable equilibrium or limit cycles. In the last few decades, research seems to have focused on continuous-time interspecific systems, rather than on the discrete-time interspecific interactions.

It is assumed that the evolution of the host population without parasitoids follows a Hassell dynamic by Hassell (1975), as given by:

$$X_{t+1} = \frac{rX_t}{\left(1 + \frac{X_T}{k}\right)^b} \tag{3}$$

where X_t is the population size in generation t ($t = 0,1,2,3,...$); a, b, and r are all positive constants; a is a scaling parameter affecting the equilibrium population size; b is a parameter to incorporate density-dependent effects such as intra-specific competition; r denotes the reproductive rate of population growth.

Leslie (1945, 1948) introduced age-structured linear population model. Consider a population divided into d age-classes or generations, which we call generations 1, 2, ..., d. Most Leslie models used for actual demographic forecasting use 5-year age groups instead of three generations. The text Matrix Population Models' by Caswell (2001) contains a comprehensive treatment of Leslie model. Leslie models with nonlinear fertility and mortality have complicated dynamical behavior. Ugarcovici and Weiss (2004) studied the dynamical behavior of Ricker model. This model is described by the two dimensional mapping $R_{a,b} : \mathbb{R}_+^2 \to \mathbb{R}_+^2$

$$R_{a,b}(x,y) = \left((ax + \gamma ay)e^{-\lambda(x+y)}, bx\right) \tag{4}$$

where x and y stand for the density of the first age group and the second age group. a and γa are the group's initial fertility rates (a, $\gamma > 0$), b is the survival rate from the first age group to the second one and λ is the decay index, $\lambda > 0$. In Eq. (4), the fertility rate monotonically decreases as a function of the total population size, the fertility decay is exponential. The other mold is Hassell model. It is described by the two dimensional mapping $H_{a,b} : \mathbb{R}^2_+ \to \mathbb{R}^2_+$

$$H_{a,b}(x,y) = \left((ax + \gamma a y)(1+x+y)^{-\beta}, bx \right) \tag{5}$$

where a and γa are the group's initial fertility rates, b is the survival rate from the first age group to the second one and β is the decay index, $\beta > 1$. In Eq. (5), the fertility rate monotonically decreases as a function of the total population size, the fertility decay is polynomial.

For some parameter values, these models admit an ergodic attractor which supports a unique physical probability measure. This physical measure satisfies in the strongest possible sense the population biologist's requirement for ergodicity in their population models. Wikan and Mjølhus (1996) and Ugarcovici and Weiss (2001) showed that Ricker mapping and Hassell mapping produce Hénon-like chaotic attractors.

Here, the local stability analysis of a discrete-time Hassell-type recruitment population model is investigated. As the parameters a, b, γ, are changed in different rang, respectively, the dynamic complexities of the model are qualitatively analyzed, and many forms of complex dynamics are observed, including chaotic bands with periodic windows, period-doubling bifurcations, Hopf and flip bifurcations, attractor crises, and non-unique dynamics (meaning that several attractors coexist). Numerical simulations are shown, including bifurcation diagrams, phase portraits, maximum Lyapunov exponents, to verify theoretical analyses and display some new and interesting nonlinear dynamical behaviors of the discrete-time system.

In biology or ecology, the complex chaotic behavior of this mapping shows the relationship between the number, birth rate and survival rate in a population, whether it survives in a balanced state or makes the population develop in disorder or chaos. This research can provide theoretical basis and help for the research in biology or ecology. For example, it is applied in the marine fishing, or in the reproduction and population growth of a certain species in nature.

2. The nonlinear Leslie population model Hassell-type

Hassell model is described by the two dimensional mapping $H_{a,b} : \mathbb{R}_+^2 \to \mathbb{R}_+^2$

$$
\begin{aligned}
x_{t+1} &= F(x_t, y_t) \\
y_{t+1} &= G(x_t, y_t)
\end{aligned}
$$

(6)

where

$$
F(x_t, y_t) = (ax_t + \gamma a y_t)(1 + x_t + y_t)^{-\beta}, \quad G(x_t, y_t) = bx_t
$$

(7)

x_t, y_t are the density of the first age group and the second one. a and γa are the group's initial fertility rates, b is the survival rate from the first age group to the second one and β is the decay index, $\beta > 1$. In Eq. (6), the fertility rate monotonically decreases as a function of the total population size, the fertility decay is polynomial.

3. Stability analysis

The Eq. (6) has one equilibrium point: $E(x^*, y^*)$, where x^*, y^* are positive and satisfy

$$
(ax^* + \gamma a y^*)(1 + x^* + y^*)^{-\beta} = x^*
$$

(8)

$$
bx^* = y^*
$$

(9)

To carry out linear stability analysis, the Taylor series expansion of Eq. (6) may be written as

$$
\begin{pmatrix} x_{t+1} \\ y_{t+1} \end{pmatrix} = \begin{pmatrix} \dfrac{\partial F}{\partial x} & \dfrac{\partial F}{\partial y} \\ \dfrac{\partial H}{\partial x} & \dfrac{\partial H}{\partial y} \end{pmatrix}_{(x^*, y^*)} \begin{pmatrix} x_t \\ y_t \end{pmatrix}
$$

(10)

Using Eq. (8) and (9), one can obtain the following:

$$
\left. \frac{\partial F}{\partial x} \right|_{(x^*, y^*)} = a(1 + x^* - \beta x^* + y^* - \beta \gamma y^*)(1 + x^* + y^*)^{-\beta-1}
$$

$$
\left. \frac{\partial F}{\partial y} \right|_{(x^*, y^*)} = a(\gamma + \gamma x^* - \beta x^* + \gamma y^* - \beta \gamma y^*)(1 + x^* + y^*)^{-\beta-1}
$$

(11)

$$
\left. \frac{\partial G}{\partial x} \right|_{(x^*, y^*)} = b
$$

$$
\left. \frac{\partial G}{\partial y} \right|_{(x^*, y^*)} = 0
$$

Consider the matrix

$$A = \begin{pmatrix} P_{11} & P_{12} \\ P_{21} & P_{22} \end{pmatrix} \tag{12}$$

where

$$P_{11} = \left.\frac{\partial F}{\partial x}\right|_{(x^*, y^*)}, \ P_{12} = \left.\frac{\partial F}{\partial y}\right|_{(x^*, y^*)}, \ P_{21} = \left.\frac{\partial G}{\partial x}\right|_{(x^*, y^*)}, \ P_{22} = \left.\frac{\partial G}{\partial y}\right|_{(x^*, y^*)} \tag{13}$$

The characteristic equation is

$$\det \begin{pmatrix} P_{11} - \lambda & P_{12} \\ P_{21} & P_{22} - \lambda \end{pmatrix} = 0 \tag{14}$$

which may be rewritten in the form

$$\lambda^2 - B\lambda + C = 0 \tag{15}$$

where

$$B = P_{11} + P_{22} = a\left(1 + x^* - \beta x^* + y^* - \beta \gamma y^*\right)\left(1 + x^* + y^*\right)^{-\beta-1}$$
$$C = P_{11}P_{22} - P_{12}P_{21} = -ab\left(\gamma + \gamma x^* - \beta x^* + \gamma y^* - \beta \gamma y^*\right)\left(1 + x^* + y^*\right)^{-\beta-1} \tag{16}$$

The roots of Eq. (15) are

$$\lambda_{1,2} = \frac{1}{2}\left(B \pm \sqrt{B^2 - 4C}\right) \tag{17}$$

Both eigenvalues are real numbers and $\left|\lambda_{1,2}\right| < 1$ if

$$B^2 - 4C > 0 \ \text{ and } \ -1 < \frac{1}{2}\left(B \pm \sqrt{B^2 - 4C}\right) < 1 \tag{18}$$

which yields

$$4C < B^2 < 4C + 4 \tag{19}$$

The eigenvalues $\lambda_{1,2}$ become complex numbers and are inside the unit circle in the complex λ -

plane for

$$B^2 - 4C < 0 \ \text{ and } \ B^2 + \left(4C - B^2\right) < 4 \tag{20}$$

which yields

6

$$B^2 < 4C < 4 \qquad (21)$$

Conditions (20) and (21) obtain when the positive equilibrium point $E(x^*, y^*)$ is stable.

4. Bifurcation analysis

As we know, Eq. (6) cannot be solved analytically, and therefore its long-term behavior must be investigated using numerical simulation. Figures 1(1-2) show the bifurcation diagrams of Eq. (6) for the density of the first age group x and the second one y with $\gamma = 0.8, \beta = 22$, b=0.7, as the parameter a increases. Because of the similarity of the bifurcation diagrams, only Figure 1(1) is shown magnified in Figure 2.

Figure 1: Bifurcation diagrams of Eq. (6): ($\gamma = 0.8, \beta = 22$, b=0.7, 0<a<45).

When the initial fertility rate a changes between 0 and 60, Eq. (6) generates complicated features. For 0<a<0.75, (0,0) is a global attractor. There exists a positive fixed point that is asymptotically stable for 0.75<a<15.8. At a=15.8, it appears a cascade of period-3 orbit. For a between 15.8 and 24, it exists a period-3 window which is embedded in strange attractor for a long time. Then each of the period-3 orbits begins to undergo a flip bifurcation, leading to chaos. The phase portraits of various a corresponding to Figure 2(1) are plotted in Figures 3(1-2). Li, York (1975) proved that if a system has period-3 point, it has all periodic points. This is also verified in the following analysis as the parameter a increasing.

When the parameter a passes through the range (24.4, 27), the bifurcation diagram in Figure 2(2) shows that this window is not a periodic window with a cascade of periodic attractors, but that it includes more complex dynamic patterns. It appears that several attractors coexist in this region: period-3 and period-5 attractors. There is a very wide chaotic band with period-6 orbit meanwhile

7

(see Figure 3(2)).

When the parameter a=27.2, the chaotic band suddenly disappears in a crisis and the system enters a periodic window with a cascade of period-doubling bifurcations leading to a chaotic attractor with periodic windows. It appears period-11 and starts to appear period-9 when the parameter a=27.24. The phase portraits which are associated with Figure 2(2) are disposed in Figures 3(2-3). When the parameter a passes through the range (27.24, 30), the detailed bifurcation diagram in Figure 2(3). As $a > 28.26$, there is a cascade of period-doubling bifurcation leading to a wide chaotic region, characterized by tangent bifurcation and attractor crises. A very narrow periodic window appears again when a=29. When a increases beyond 28.5, a chaotic attractor abruptly appears and the periodic attractor disappears. The chaotic band has changed into four chaotic bands. This kind of transilienc of chaotic state caused by the continuous change of parameters is called chaos crisis by Grebogi (1983). Because the unstable periodic orbit meets the secondary chaotic band, the orbits in the chaotic band is filled between all levels of orbits, leading to the emergence of chaos crisis. The phase portraits of various a corresponding to Figure 2(3) are plotted in Figures 3(4-6). When the parameter a passes through the range (30.8, 31.7) in Figure. 2(4), a large periodic window appears, then chaos appears because of period-doubling bifurcation. When the parameter a=49, it appears period-4, and it appears period-9 at a=51.2, at last the Eq. (6) appears a chaotic attractor. The phase portraits which are associated with Figure 2(5) are disposed in Figures 3(7-8).

From the above analysis, it can be seen that the two-dimensional nonlinear mapping is a process of intermittently breaking up in accordance with periodic behavior and chaos phenomenon, so that the system appears chaotic motion state, which is called Pomeau-Manneville path (through intermittence chaos) by Eckmann (1981). In the process of parameter change, when the periodic window appears, the one of the roots of Eq. (14) is -1. The unstable period doubling bifurcation

happens immediately, and the periodic point becomes the periodic saddle point. Once the mapping point falls near the unstable periodic point, it will leave along the unstable manifold, and chaos will appear. Eq. (6) also contains Feigenbaum path (through fork bifurcation) to chaos.
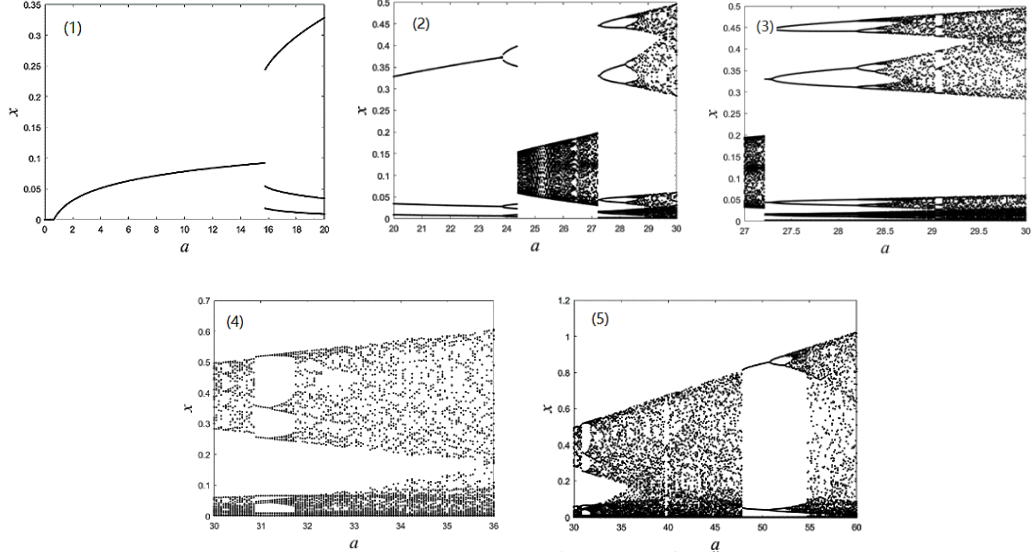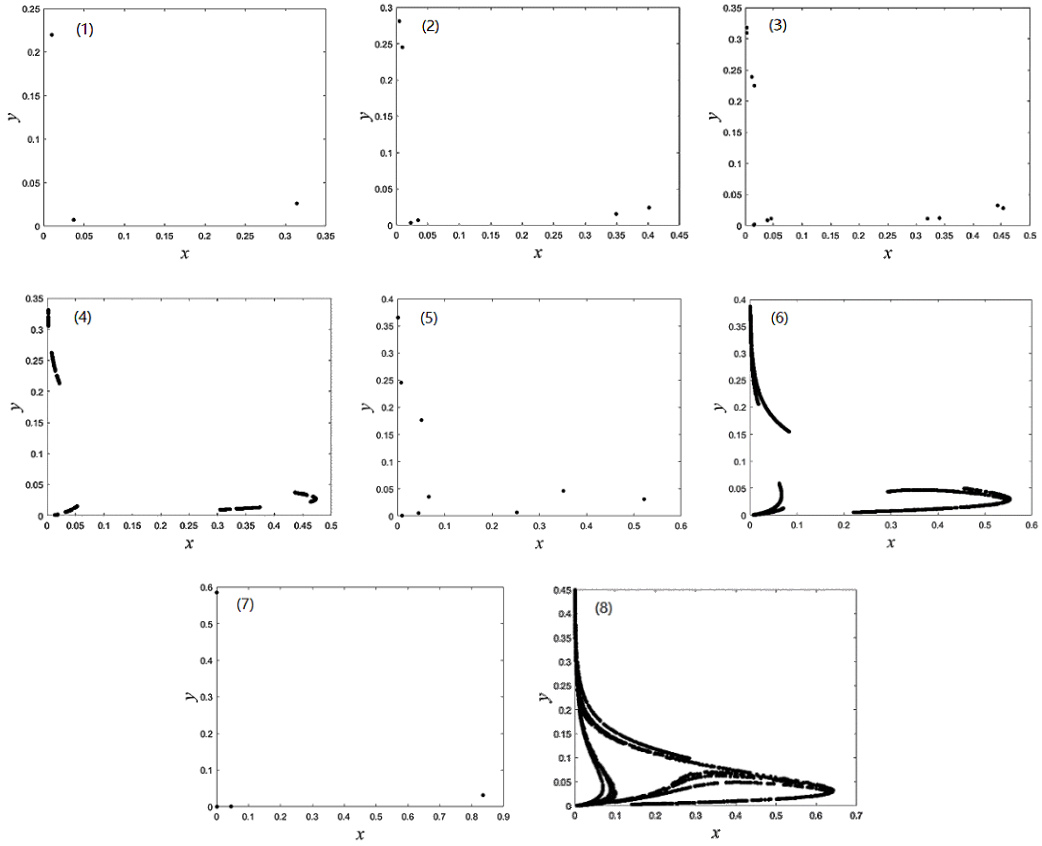

Figure 2: Magnification of part of Figure 1(1).

Figure 3: The phase diagrams of Eq. (6): ((1)15.8<a<24, (2) 22.4<a<27,

9

(3) $a=27.4$,(4-6) $28.26<a<30.8$, (7-8) $30.8<a<60$).

Figures 4(1-2) show the bifurcation diagrams of Eq. (6) for the density of the first age group x and the second one y with $\gamma = 0.8, \beta = 22$, $a=38$, as the parameter b increases. Figures 4(3-5) are the graphs magnified of Figures 4(1-2).
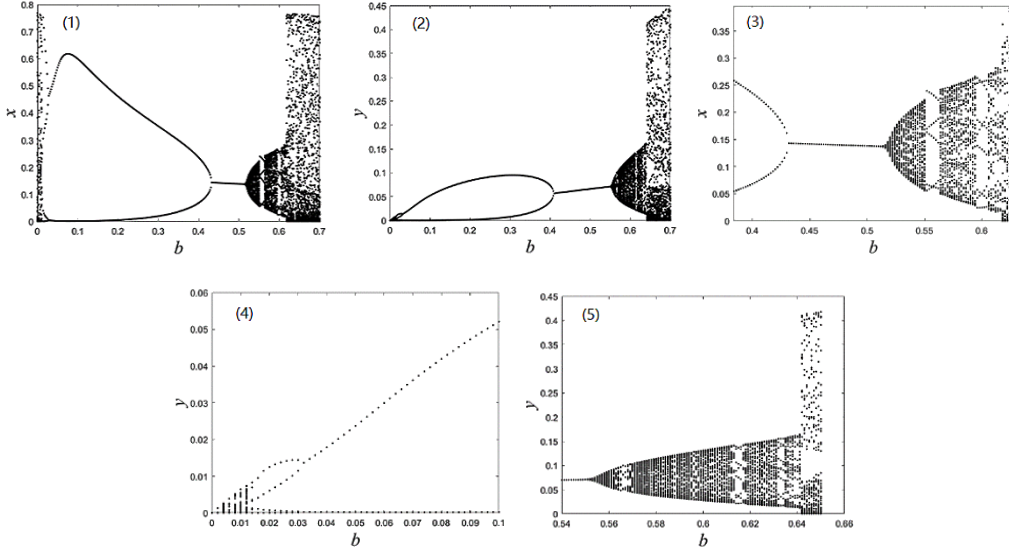

Figure 4: Bifurcation diagrams of Eq. (6): ($\gamma = 0.8, \beta = 22$, $a=38$, $0<b<0.7$).

In Figure 4(1), as the parameter b increases from 0 to 0.03, a narrow chaotic band appears. When the parameter $b = 0.03$, the chaotic regime suddenly disappears in a crisis and the system appears a period-2 orbit for $b\in(0.03, 0.435)$, and a stable fixed point for $b\in(0.435, 0.526)$. A flip bifurcation occurs at $b = 0.435$. Figure 5(1) presents the phase portrait of period-2. As the parameter $b\in(0.526, 0.55)$ in Figure 4(3), the Eq. (6) goes through a quasi-periodic region (including tangent bifurcation, narrow and wide periodic windows, and frequency lockings which appear as a collapse of the invariant circle to a periodic orbit). We can see that there is a stable fixed point for $b<0.526$, and the fixed point loses its stability as b increases. A Hopf bifurcation occurs at $b=0.526$ and an attracting invariant cycles bifurcates from the fixed point. In this case, Eq. (14) has two conjugate complex roots λ and $\bar{\lambda}$, satisfying $\left|\lambda\bar{\lambda}\right|=1$.

10

As b is increasing, the smooth invariant loop becomes larger and no longer smooth. At last, the invariant loop breaks. As b=0.59, there is a cascade of period-doubling bifurcation leading to a wide chaotic region, characterized by tangent bifurcation and attractor crises. Further, when $b \in (0.55, 0.56)$ and $b \in (0.592, 0.614)$, we can observe the period-5, 8 windows within the chaotic regions, respectively. The phase portraits of various b corresponding to Figure 4 (3) are plotted in Figures 5(2-6).

In the same way as research the dynamics in (a, x) plane, we investigate the dynamics in (a, y) plane with the same parameters.

In Figure 4(4), as the parameter b increases from 0 to 0.01, a narrow chaotic band appears. We can observe that there are period-3 orbit for $b \in (0.01, 0.03)$ and a period-2 orbit for $b \in (0.03, 0.4)$. There is a stable fixed point for $b \in (0.41, 0.553)$. A flip bifurcation occurs at $b = 0.41$ in Figure 4(2). In Figure 4(5), a Hopf bifurcation occurs at b=0.553 and an attracting invariant cycles bifurcates from the fixed point. As the parameter $b \in (0.553, 0.64)$, the Eq. (6) goes through a quasi-periodic region including tangent bifurcation, narrow and wide periodic windows, and frequency lockings. Further, we can observe that several different periodic windows are embedded in this region respectively. There is a cascade of period-doubling bifurcation leading to a wide chaotic region, characterized by tangent bifurcation and attractor crises.

According to the above analysis, when the parameter b is increasing, chaos appears by the Ruelle Takens Newhouse scheme (through Hopf bifurcation) and the Pomeau-Manneville path (through intermittence chaos). In the larger region of the control parameter space, the path leading to chaos is related to the Hopf bifurcation. In these ways, the locking phase and quasi-periodic motion can be observed.
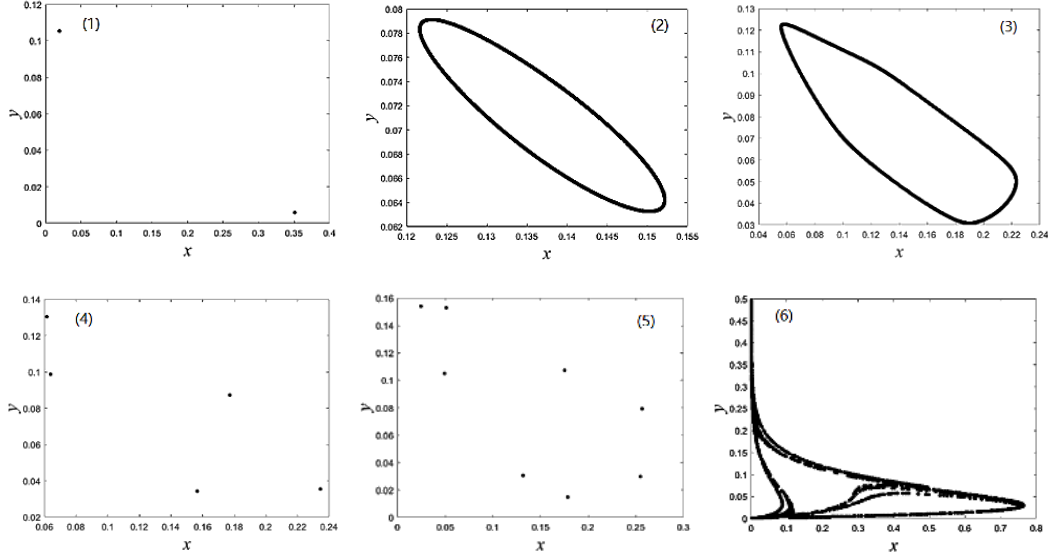
Figure 5: The phase diagrams of Eq. (6): ((1)0.03<b<0.435, (2-3) 0.526<a<0.59,

(4) 0.55<b<0.56, (5) 0.592<b<0.614, (6) b>0.614).

Figure 6(1) shows the bifurcation diagram of Eq. (6) for the density of the first age group x with $a=38, b=0.7, \beta=22$ as the parameter γ increases. Figure 6(2) is the graph magnified of Figure. 6(1).
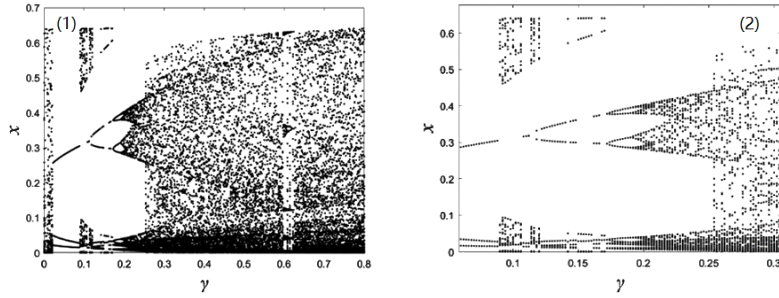

Figure 6: Bifurcation diagrams of Eq. (6): ($\beta=22$, $a=38$, b=0.7, $0<\gamma<0.8$).

In Figure 6(1), as the parameter γ increases from 0 to 0.03, a narrow chaotic band appears. When the parameter $\gamma=0.03$, the chaotic band suddenly disappears in a crisis and the system enters a periodic window. Figure 7(1) presents the phase portrait as $\gamma \in (0, 0.03)$. We can observe that there are period-3 orbit for $\gamma \in (0.03, 0.08)$, and two chaotic bands with periodic windows for $\gamma \in (0.08, 0.125)$. It shows that the existence of period-3 means that there are any periodic points, and finally

chaos appears. Figure 7(2) presents the phase portrait of period-3. At $\gamma = 0.125$, the chaotic band

suddenly disappears in a crisis and the Eq. (6) enters a periodic window with a cascade of period-

doubling bifurcations. A flip bifurcation and an inverted bifurcation occur. At $\gamma = 0.158$, there is

period-6 orbit. At $\gamma = 0.175$, there is a cascade of period-doubling bifurcation leading to three chaotic

bands, characterized by tangent bifurcation and attractor crises. The phase portraits of various γ

corresponding to Figures 6 (1-2) are plotted in Figures 7(3-5).

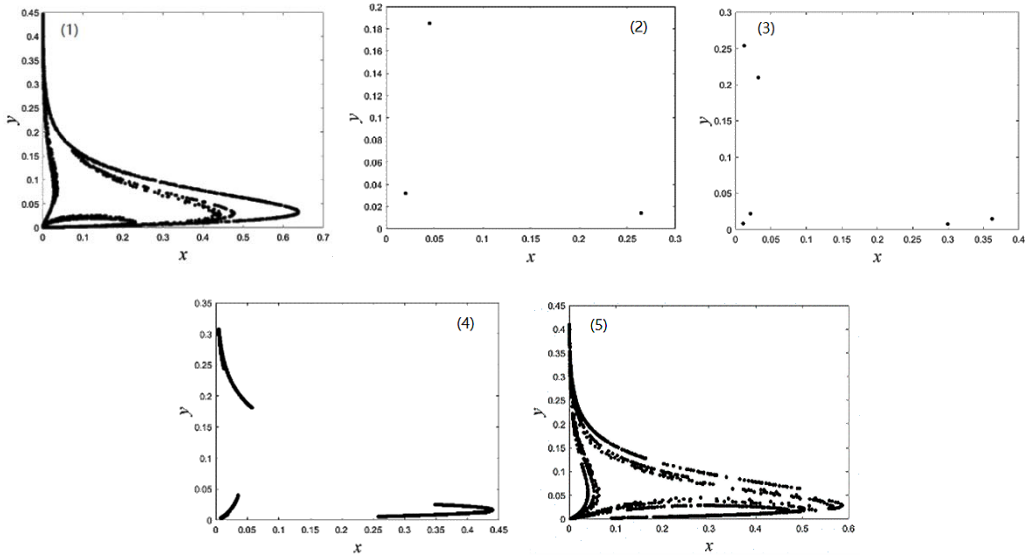Figure 7: The phase diagrams of Eq. (6): ((1) $0<\gamma<0.03$, (2) $0.03<\gamma<0.08$,

(3) $\gamma=0.158$, (4) $\gamma=0.75$, (5) $\gamma>0.25$).

5. The largest Lyapunov exponent

In this section, the largest Lyapunov exponent, which has proven to be the most useful dynamic

diagnostic tool for chaotic systems, is considered. This quantity represents the average exponential

rate of divergence or convergence of nearby orbits in phase space [18]. The general approach for

calculating the largest Lyapunov exponent is to follow two nearby orbits and to calculate their

average logarithmic rate of separation. Whenever they move too far apart, one of the orbits has to

be moved back to the vicinity of the other along the line of separation. For a chaotic attractor, the

largest Lyapunov exponent LE_{max} must be positive. If LE_{max} is negative, this implies a stable state or a periodic attractor.

The largest Lyapunov exponents corresponding to the cases shown in Figures 1, 4, and 6 have been calculated and plotted in Figures 8(1-3), respectively. The existence of chaotic regions in the parametric space is clearly visible in these Figures. The largest Lyapunov exponents for the strange attractors were found to be LE_{max} = 12.21, 19.81, and 17.35, respectively.

In Figure 8(1), we can easily see that the maximum Lyapunov exponents are negative for the parameter $a \in (0, 25.5)$, that is to say, the Eq. (6) has no chaotic region. For $a \in (25.5, 35)$, some Lyapunov exponents are bigger than 0, some are smaller than 0, so there exists stable fixed point or stable periodic windows in the chaotic region. In Figure 8(2), the maximum Lyapunov exponents are positive for the parameter $b \in (0, 0.03)$, that is to say, the Eq. (6) appears a chaotic region. For $b \in (0.03, 0.526)$, the maximum Lyapunov exponents are negative, the Eq. (6) appears periodic. For $b \in (0.526, 0.7)$, some Lyapunov exponents are bigger than 0, some are smaller than 0, so there exist periodic windows in the chaotic region. In Figure 8(3), the maximum Lyapunov exponents are positive for the parameter $\gamma \in (0, 0.158)$ and $\gamma \in (0.28, 0.8)$, the Eq. (6) appears a chaotic region. For $\gamma \in (0.158, 0.28)$, the maximum Lyapunov exponents are negative, the Eq. (6) appears periodic.

We find that the analysis of the maximum Lyapunov exponents is consistent with the dynamic properties of the system under different parameters.
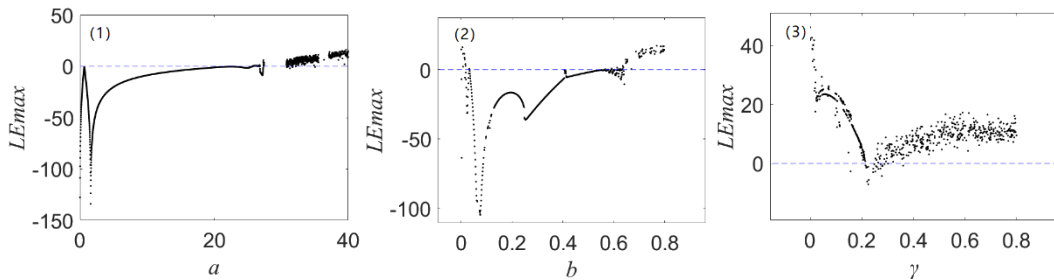

Figure 8: (1)Lyapunov exponent of Eq. (6) with $\gamma = 0.8, \beta = 22$, b=0.7, 0<a<40;

(2)Lyapunov exponent of Eq. (6) with $\gamma = 0.8, \beta = 22$, a=38, 0<*b*<0.7;

(3)Lyapunov exponent of Eq. (6) with $\beta = 22$, *a*=38, *b*=0.7, $0 < \gamma < 0.8$.

6. Concluding

A discrete-time Leslie model with Hassell growth function for two generations is investigated by qualitative analysis and numerical simulation. Local stability analysis of the system is carried out. Many forms of complex dynamics are observed, including chaotic bands with periodic windows, flip bifurcations, and Hopf bifurcations, attractor crises, and non-unique dynamics (meaning that several attractors coexist). Numerical simulation results not only show the consistence with the theoretical analysis but also display the new and interesting dynamical behaviors, including different periodic orbits in chaotic regions, attracting invariant circle, period-doubling bifurcations from stable equilibriums leading to chaos, interior crisis and boundary crisis. The largest Lyapunov exponents are numerically computed to confirm further the complexity of these dynamic behaviors.

In biology or ecology, the complex chaotic behavior of this mapping shows the relationship between the number, birth rate and survival rate in a population, whether it survives in a balanced state or makes the population develop in disorder or chaos. This research can provide theoretical basis and help for the research in biology or ecology. For example, it is applied in the marine fishing, or in the reproduction and population growth of a certain species in nature.

Data Accessibility Statement: No data, models, or code were generated or used during the study.

References

[1] Verhulst P. F. (1838). Notice sur la loi que la population suit dans son accroissement. *Corr. Math. Phys*, *10*: 113–21.

[2] Pearl R., Reed L. J. (1920). On the rate of growth of the population of the United States since 1790 and its mathematical representation. *Proc. Natl. Acad. Sci.*, *6*: 275–88.

[3] Leslie P. (1945). On the use of matrices in population mathematics. *Bio. Metrika*, *33*: 183–212.

[4] Leslie P. (1948). Some further notes on the use of matrices in population mathematics. *Bio. Metrika*, *35*: 213–245.

[5] Lorenz E. N. (1963). Deterministic non periodic flow. *Atmos. Sci.*, *20*: 130–141.

[6] Tianyan-Li, Yorke J. A. (1975). Period three implies chaos. *Amer. Math. Monthly*, *82*: 985–992.

[7] Beddington J. R., Free C. A., Lawton J. H. (1975). Dynamic complexity in predator–prey models framed in difference equations. *Nature*, *255*: 58–60.

[8] Hassell M. P. (1975). Density-dependence in single species populations. *J. Animal. Ecol.*, *44*: 283–295.

[9] Smale S. (1976). Differentiable dynamical systems. *Bull. Amer. Soc.*, *73*: 747–817.

[10] May R. M. (1976). Simple mathematical models with very complicated dynamics. *Nature*, *261*: 459–67.

[11] Lasota A. (1981). Stable and chaotic solution sofa first order partial differential equation. *Nonlinear Analysis*, *7*(11): 1181–1193.

[12]Eckmann J. P. (1981). Roads to turbulence in dissipative dynamics system. *Rev. Mod. Phys*., *53*: 643–649.

[13] Grebogi C., Ott E., Yorke J. A. (1983). Crisis, sudden changes in chaotic attractors, and transient chaos. *Phys.*, *7*D: 181–188.

[14] Brunovsky P. (1983). Notes on chaos in the cell population partial differential equation. *Nonlinear Analysis*, *7*(2): 167–176.

[15] Rosenstein M. T., Collins J. J., De Luca C. J. (1993). A practical method for calculating largest Lyapunov exponents from small data sets. *Phys. D*, *65*: 117–3.

[16] Wikan A. and Mjølhus E. (1996). Over compensatory recruitment and generation delay in discrete age-structured population models. *J. Math. Biol.*, *35*: 195–239.

[17] Caswell H. (2001). *Matrix Population Models*. (2nd Edition) (Sunderland, MA: Sinauer).

[18] IIie Ugarcovici and Weiss H. (2004). Chaotic dynamics of a nonlinear density dependent population model. *Nonlinearity*, *17*: 1689–1711.